Electronic Supplementary Information

Facile C−N coupling of coordinated ammonia and labile carbonyl or acetonitrile promoted by a thiolate-bridged dicobalt reaction scaffold

Jianzhe Li,[a] Dawei Yang,*[a] Peng Tong,[a] Baomin Wang[a] and Jingping Qu*[ab]

[a]*State Key Laboratory of Fine Chemicals, Dalian University of Technology, Dalian 116024, P. R. China*

[b]*Key Laboratory for Advanced Materials, East China University of Science and Technology, Shanghai 200237, P. R. China*

*E-mail: qujp@dlut.edu.cn

yangdw@dlut.edu.cn

Table of Contents

I. X-ray crystallographic data

Table S1 Crystallographic data for **2** and **3**·2CH_2Cl_2.

	2	**3**·2CH_2Cl_2
Formula	$C_{25}H_{42}Co_2INOS_2$	$C_{26}H_{47}Cl_4Co_2I_2NS_2$
Formula weight	681.47	951.22
Crystal dimensions (mm^3)	0.28×0.26×0.25	0.30×0.24×0.23
Crystal system	Triclinic	Monoclinic
Space group	P−1	P2(1)/n
a (Å)	8.5554(4)	12.1666(5)
b (Å)	11.8305(5)	15.2586(6)
c (Å)	14.1576(6)	19.7131(7)
α (°)	75.2970(14)	90
β (°)	86.9868(14)	93.8173(10)
γ (°)	88.2112(13)	90
Volume ($Å^3$)	1383.88(11)	3651.5(2)
Z	2	4
T (K)	173(2)	173(2)
D_{calcd} (g cm^{-3})	1.635	1.730
μ (mm^{-1})	2.483	3.024
F (000)	692	1880
No. of rflns. collected	17695	76910
No. of indep. rflns. /R_{int}	4828/0.0334	6413/0.0278
No. of obsd. rflns. [$I_0 > 2\sigma(I_0)$]	4629	5928
Data / restraints / parameters	4828/0/297	6413/0/346
R_1 / wR_2 [$I_0 > 2\sigma(I_0)$]	0.0277/0.0755	0.0305/0.0852
R_1 / wR_2 (all data)	0.0288/0.0764	0.0341/0.0878
GOF (on F^2)	0.924	1.062
Largest diff. peak and hole (e $Å^{-3}$)	0.651/−0.650	0.958/−1.614
CCDC No.	1990564	1990565

Table S2 Crystallographic data for **4**·MeCN and **5**.

	4·MeCN	**5**
Formula	$C_{28}H_{49}Co_2F_{12}N_3P_2S_2$	$C_{26}H_{45}Co_2F_6N_2PS_2$
Formula weight	899.62	712.59
Crystal dimensions (mm^3)	0.28×0.25×0.24	0.32×0.28×0.26
Crystal system	Orthorhombic	Monoclinic
Space group	Pbca	P2(1)/n
a (Å)	17.1790(8)	8.565(2)
b (Å)	14.6705(7)	28.994(7)
c (Å)	30.3404(14)	12.607(3)
α (°)	90	90
β (°)	90	92.037(5)
γ (°)	90	90
Volume ($Å^3$)	7646.5(6)	3128.9(13)
Z	8	4
T (K)	173(2)	296(2)
D_{calcd} ($g\ cm^{-3}$)	1.563	1.513
μ (mm^{-1})	1.144	1.300
F (000)	3696	1480
No. of rflns. collected	56387	54174
No. of indep. rflns. /R_{int}	9007/0.0543	5508/0.0284
No. of obsd. rflns. [$I_0 > 2\sigma(I_0)$]	7527	4982
Data / restraints / parameters	9007/0/456	5508/0/344
R_1 / wR_2 [$I_0 > 2\sigma(I_0)$]	0.0548/0.1508	0.0415/0.1110
R_1 / wR_2 (all data)	0.0661/0.1588	0.0467/0.1138
GOF (on F^2)	1.025	1.019
Largest diff. peak and hole (e $Å^{-3}$)	1.336/−0.979	0.675/−0.482
CCDC No.	1990566	1990567

Fig. S1 ORTEP diagram of **2**. The thermal ellipsoids were shown at 50% probability level. Hydrogen atoms on carbons and one I anion are omitted for clarity.

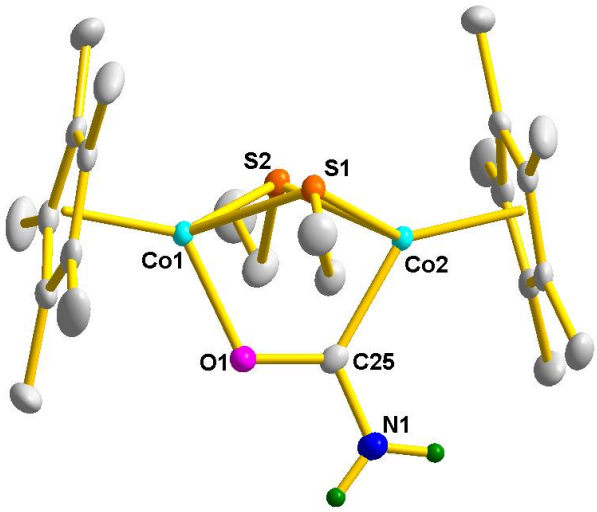

Table S3 Selected bond distances (Å) and angles (°) for **2**.

Distances (Å)			
Co1···Co2	3.0888(1)	Co1–S1	2.2543(7)
Co1–S2	2.2664(7)	Co2–S1	2.2308(7)
Co2–S2	2.2440(7)	Co1–O1	1.9401(19)
Co2–C25	1.926(3)	C25–O1	1.284(3)
C25–N1	1.329(4)	Co1–Cp*1	1.6851(1)
Co2–Cp*2	1.7117(1)		
Angles (º)			
Co1–S1–Co2	87.05(3)	Co1–S2–Co2	86.44(3)
S1–Co1–S2	81.80(3)	S1–Co2–S2	82.82(3)
Co1–O1–C25	115.92(17)	Co2–C25–N1	126.5(2)
Co2–C25–O1	119.8(2)	N1–C25–O1	113.8(3)
Torsion angles (°)			
S1–Co1Co2–S2	129.736(2)		
Dihedral angles (°)			
Cp*1–Cp*2	23.529		

Fig. S2 ORTEP diagram of **3**·2CH_2Cl_2. The thermal ellipsoids were shown at 50% probability level. Hydrogen atoms on carbons, two co-crystallized CH_2Cl_2 molecules and one I anion are omitted for clarity.

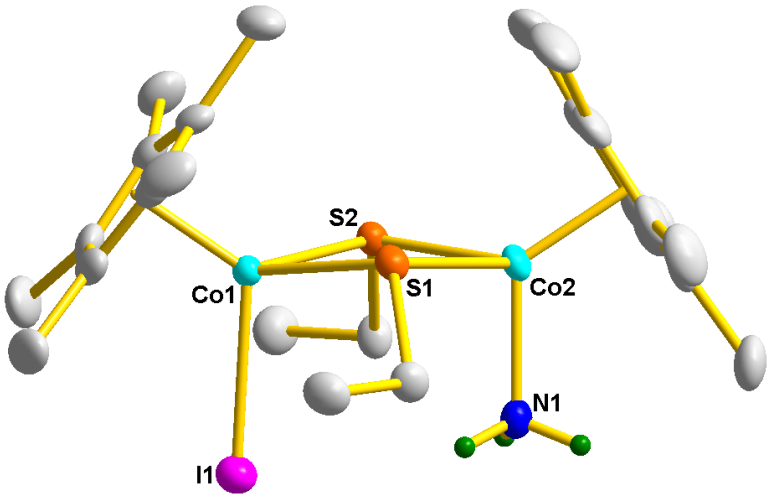

Table S4 Selected bond distances (Å) and angles (°) for **3**·2CH_2Cl_2.

Distances (Å)			
Co1···Co2	3.4102(1)	Co1–S1	2.2773(10)
Co1–S2	2.2631(10)	Co2–S1	2.2633(10)
Co2–S2	2.2534(10)	Co1–I1	2.5883(5)
Co2–N1	1.976(3)	Co1–Cp*1	1.7231(1)
Co2–Cp*2	1.7060(1)		
Angles (°)			
Co1–S1–Co2	97.36(4)	Co1–S2–Co2	98.06(4)
S2–Co1–S1	81.11(3)	S1–Co2–S2	81.62(3)
Torsion angles (°)			
S1–Co1Co2–S2	164.402(2)		
Dihedral angles (°)			
Cp*1–Cp*2	69.021		

Fig. S3 ORTEP diagram of **4**·MeCN. The thermal ellipsoids shown were at 50% probability level. Hydrogen atoms on carbons, one co-crystallized MeCN molecule and two PF_6 anions are omitted for clarity.

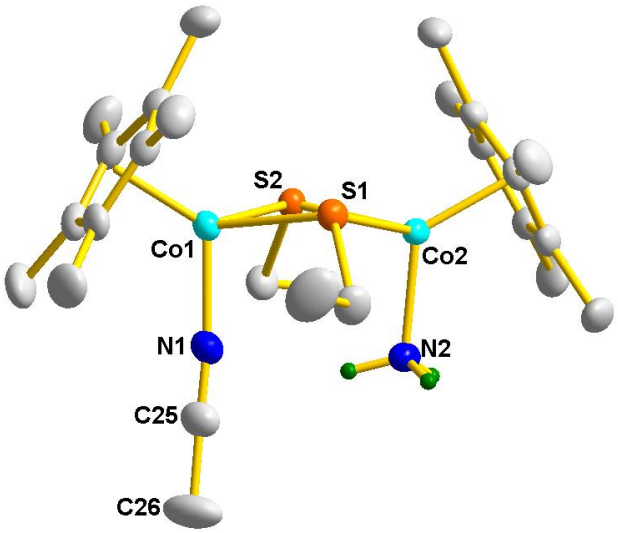

Table S5 Selected bond distances (Å) and angles (°) for **4**·MeCN.

Distances (Å)			
Co1···Co2	3.3949(1)	Co1–S1	2.2605(9)
Co1–S2	2.2535(9)	Co2–S1	2.2605(9)
Co2–S2	2.2626(9)	Co1–N1	1.923(3)
Co2–N2	1.987(3)	N1–C25	1.142(5)
Co1–Cp*1	1.7061(1)	Co2–Cp*2	1.7039(1)
Angles (°)			
Co1–S1–Co2	97.34(3)	Co1–S2–Co2	97.48(3)
S2–Co1–S1	80.47(3)	S1–Co2–S2	80.28(3)
Co1–N1–C25	173.4(3)		
Torsion angles (°)			
S1–Co1Co2–S2	155.837(3)		
Dihedral angles (°)			
Cp*1–Cp*2	61.921		

Fig. S4 ORTEP diagram of **5**. The thermal ellipsoids were shown at 50% probability level. Hydrogen atoms on carbons and one PF_6 anion are omitted for clarity.

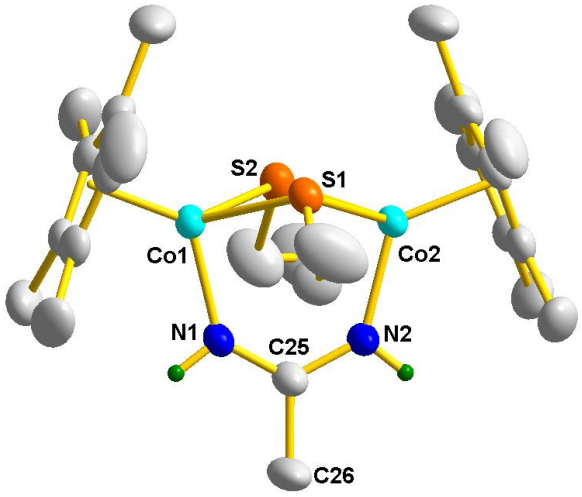

Table S6 Selected bond distances (Å) and angles (°) for **5**.

Distances (Å)			
Co1···Co2	3.2296(5)	Co1–S1	2.2446(10)
Co1–S2	2.2454(10)	Co2–S1	2.2576(10)
Co2–S2	2.2458(10)	Co1–N1	1.924(3)
Co2–N2	1.920(3)	N1–C25	1.305(4)
N2–C25	1.320(4)	C25–C26	1.506(5)
Co1–Cp*1	1.6977(3)	Co2–Cp*2	1.7065(3)
Angles (°)			
Co1–S1–Co2	91.67(3)	Co1–S2–Co2	91.96(4)
S2–Co1–S1	82.50(3)	S1–Co2–S2	82.20(3)
Co1–N1–C25	132.6(3)	Co2–N2–C25	131.8(3)
N1–C25–N2	123.3(3)	N1–C25–C26	118.6(3)
N2–C25–C26	118.1(3)		
Torsion angles (°)			
S1–Co1Co2–S2	142.215(11)		
Dihedral angles (°)			
Cp*1–Cp*2	42.786		

II. NMR spectra

Fig. S5 The ^{1}H NMR spectrum of **2** in CD_2Cl_2.

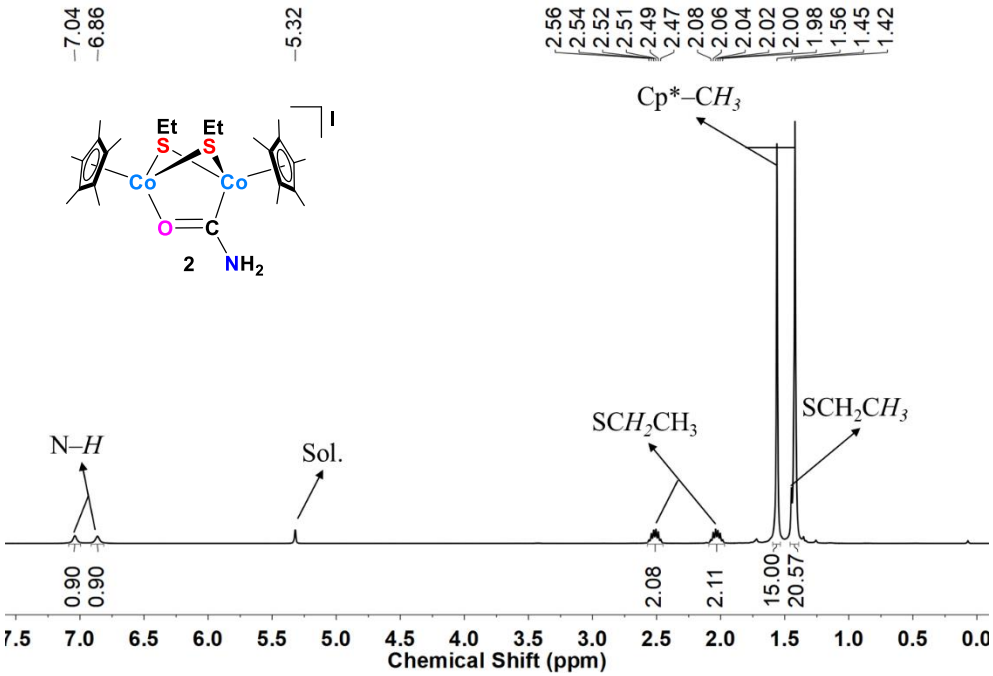

Fig. S6 The ^{13}C NMR spectrum of **2** in CD_2Cl_2.

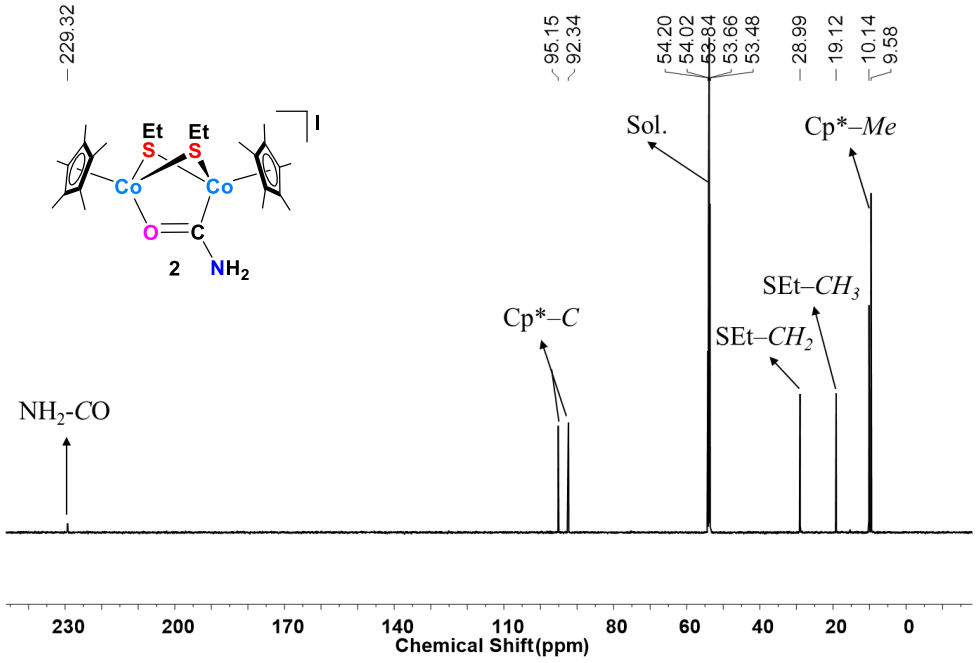

Fig. S7 The ^{1}H NMR spectrum of **3** in CD_2Cl_2.

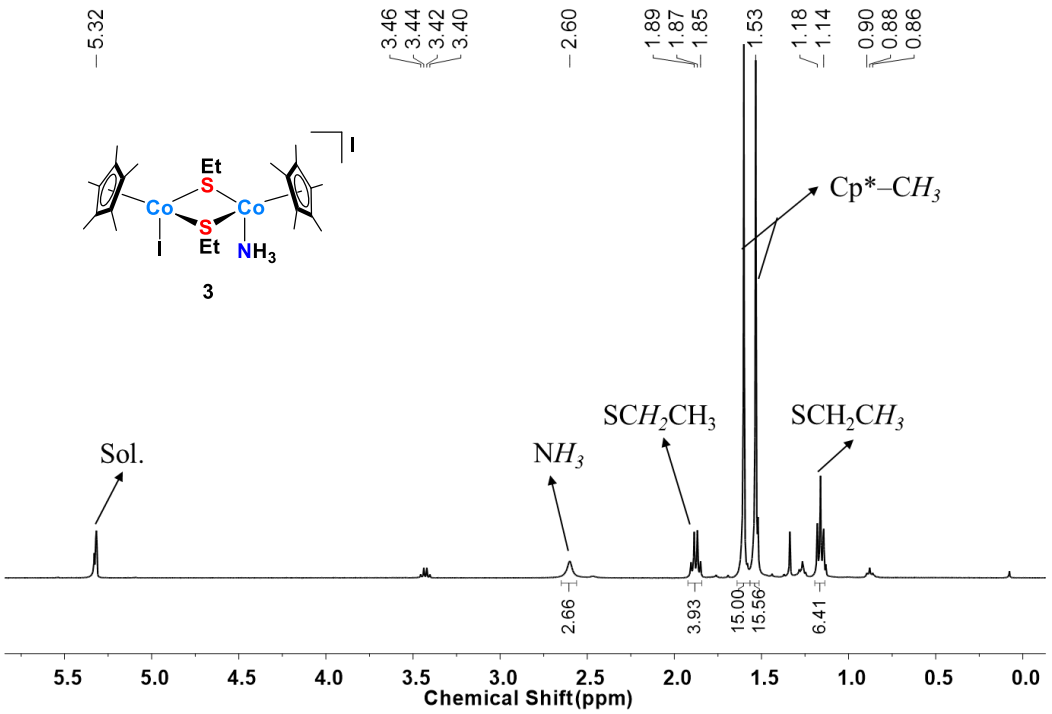

Fig. S8 The ^{13}C NMR spectrum of **3** in CD_2Cl_2.

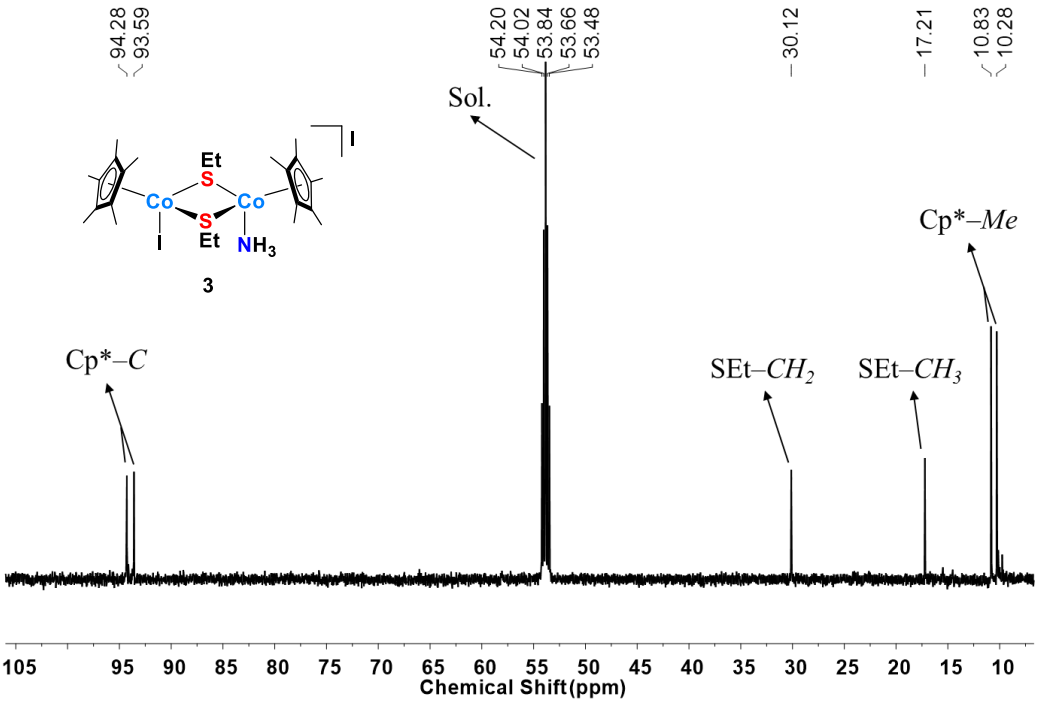

Fig. S9 The ^{1}H NMR spectrum of **4** in CD_2Cl_2.

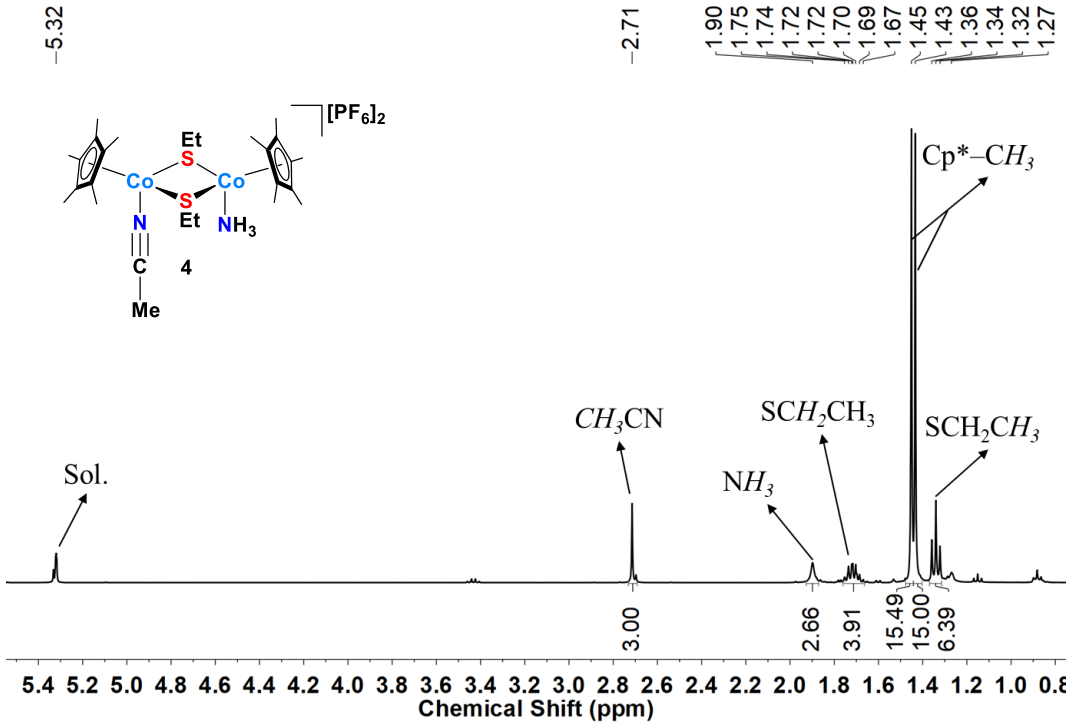

Fig. S10 The ^{1}H NMR spectrum of D-**4** in CD_2Cl_2.

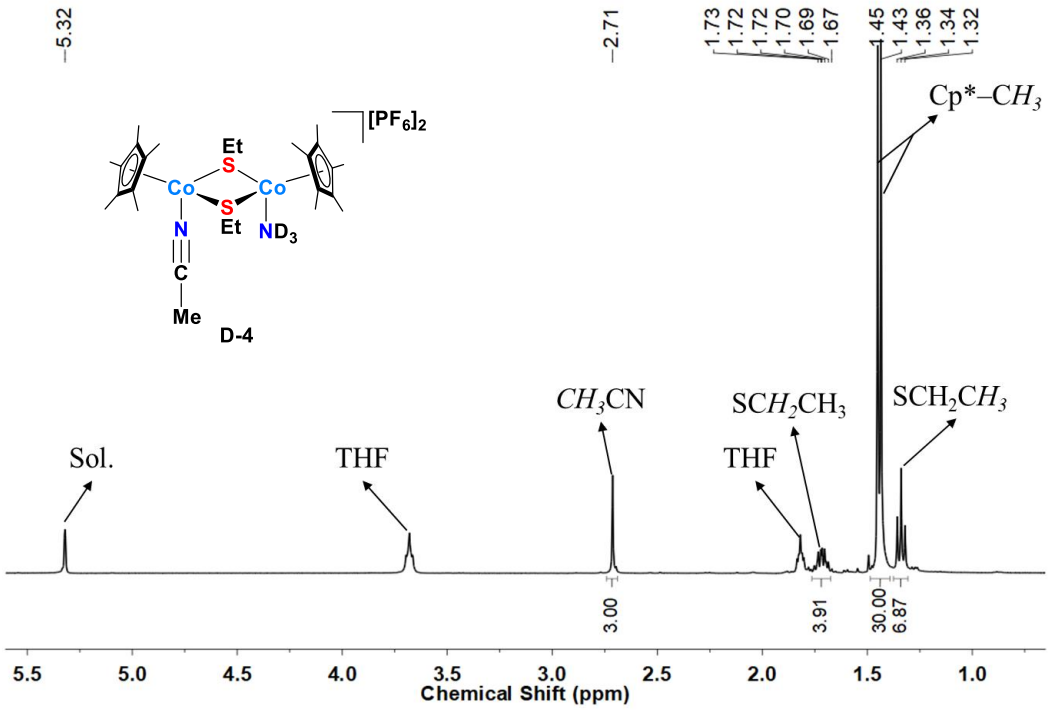

Fig. S11 The ^{13}C NMR spectrum of **4** in CD_2Cl_2.

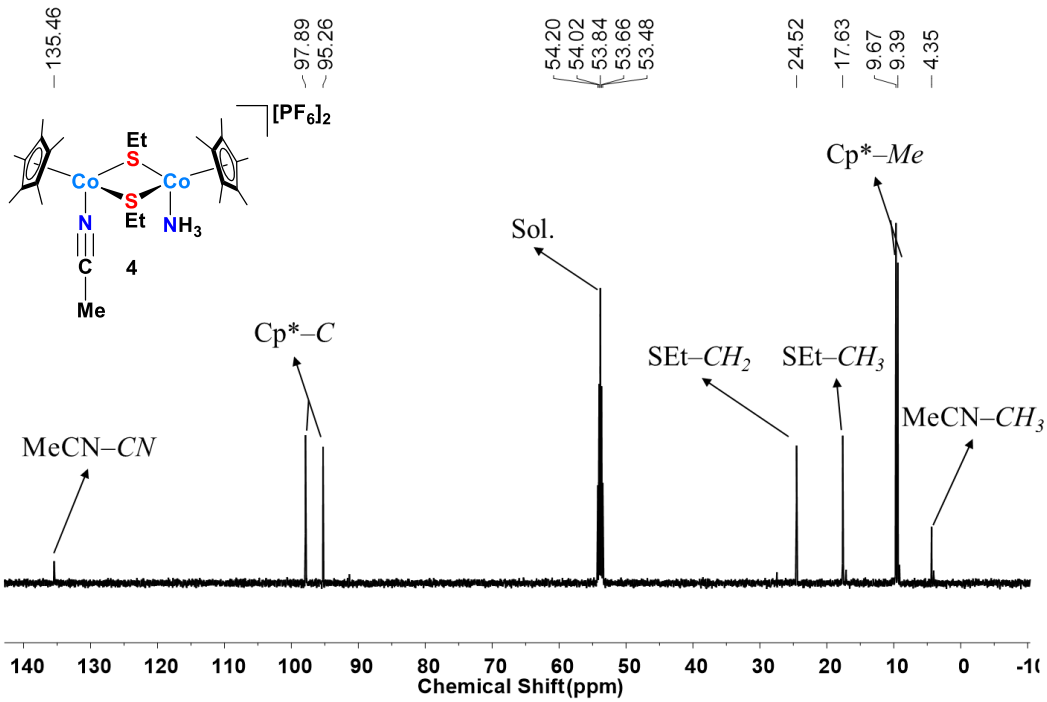

Fig. S12 The ^{1}H NMR spectrum of **5** in CD_2Cl_2.

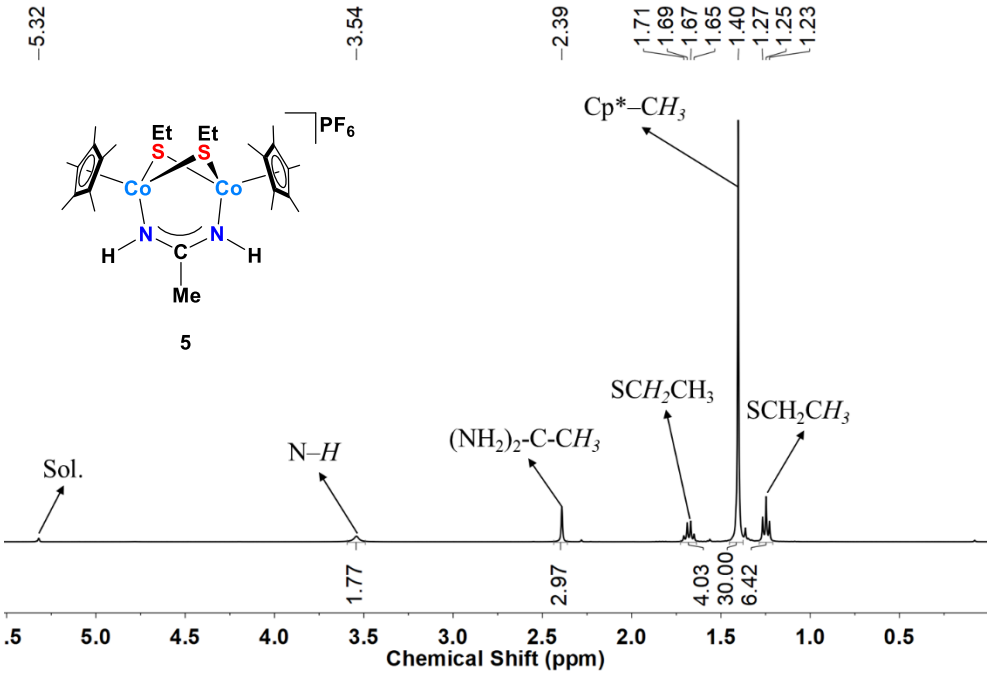

Fig. S13 The ^{13}C NMR spectrum of **5** in CD_2Cl_2.

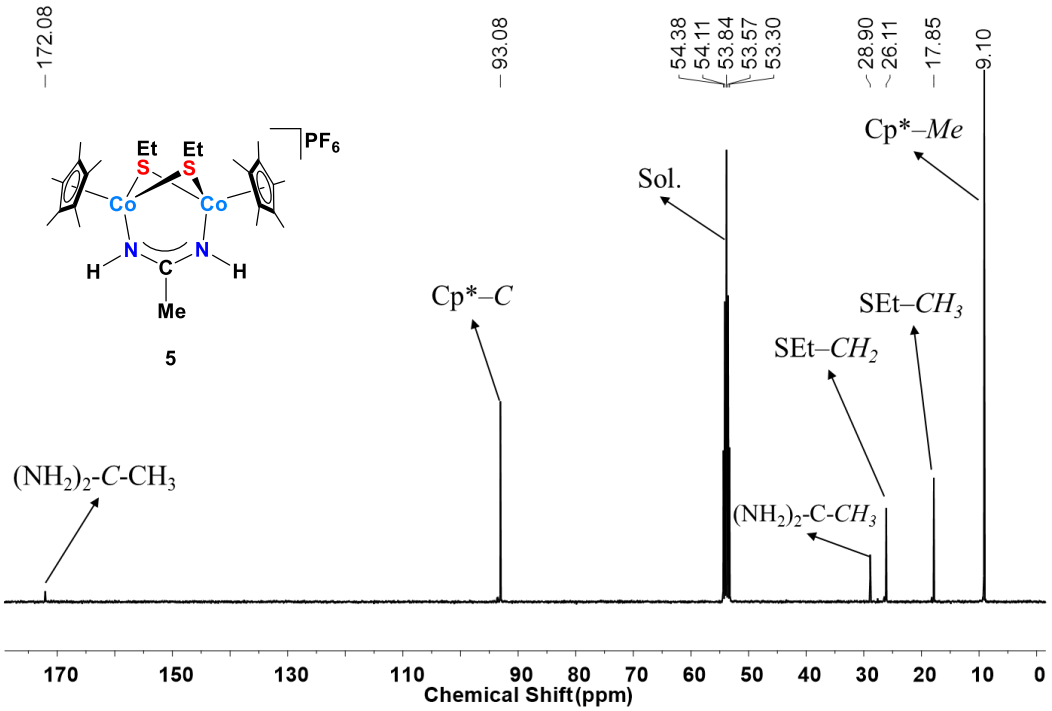

Fig. S14 The ^{1}H NMR spectrum of the product from the reaction of complex **5** with HBF_4 in CD_2Cl_2.

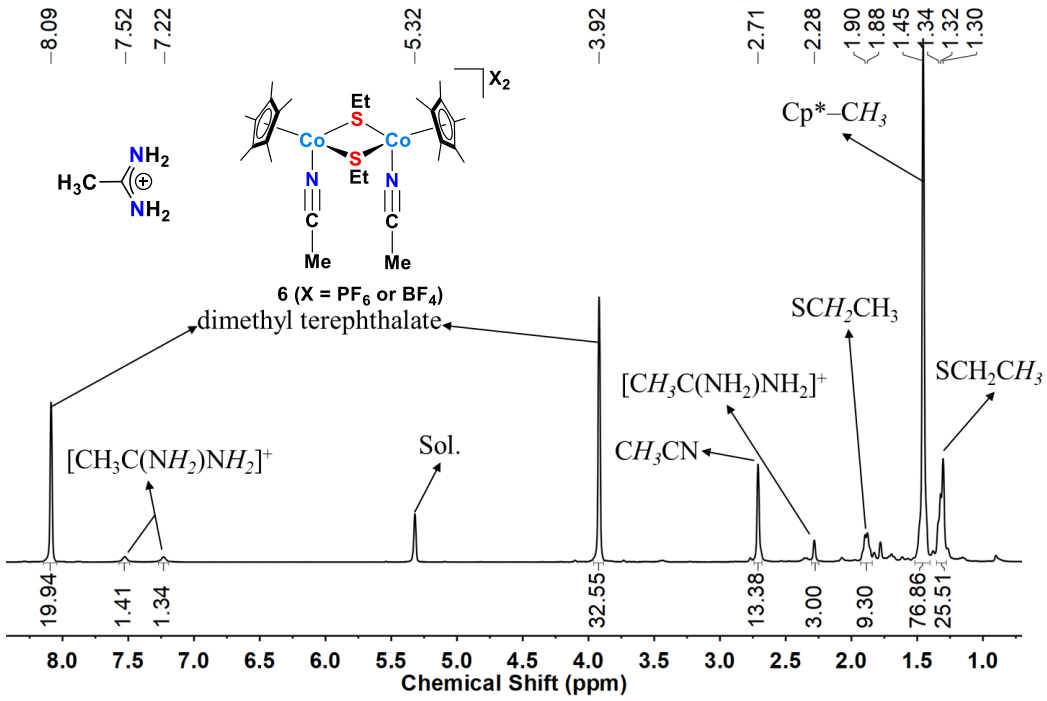

III. ESI-HRMS

Fig. S15 ESI-HRMS of **2** in CH_2Cl_2.

(a) The signal at *m/z* = 554.1376 corresponds to $[\mathbf{2}-I]^+$. (b) Calculated isotopic distribution for $[\mathbf{2}-I]^+$ (upper) and the amplifying diagram for $[\mathbf{2}-I]^+$ (bottom).

(a)

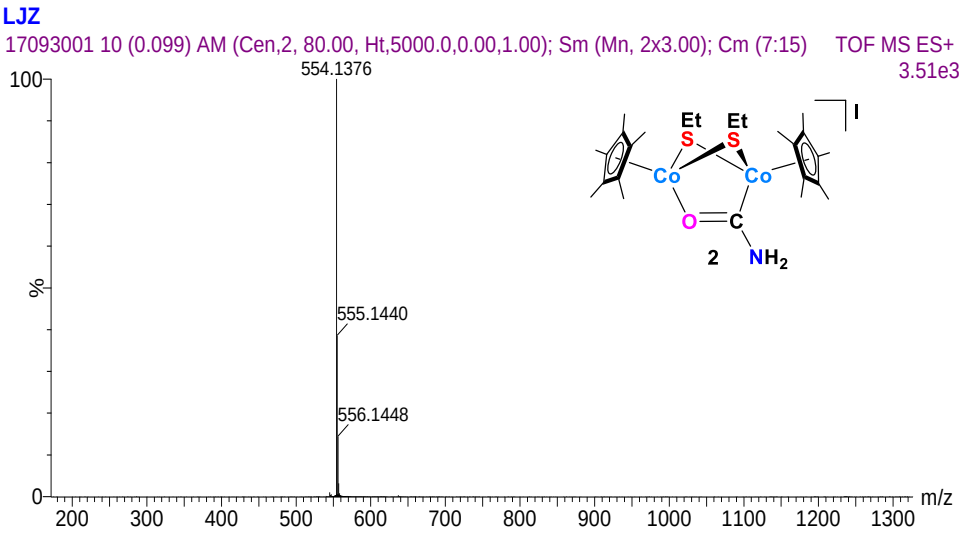

(b)

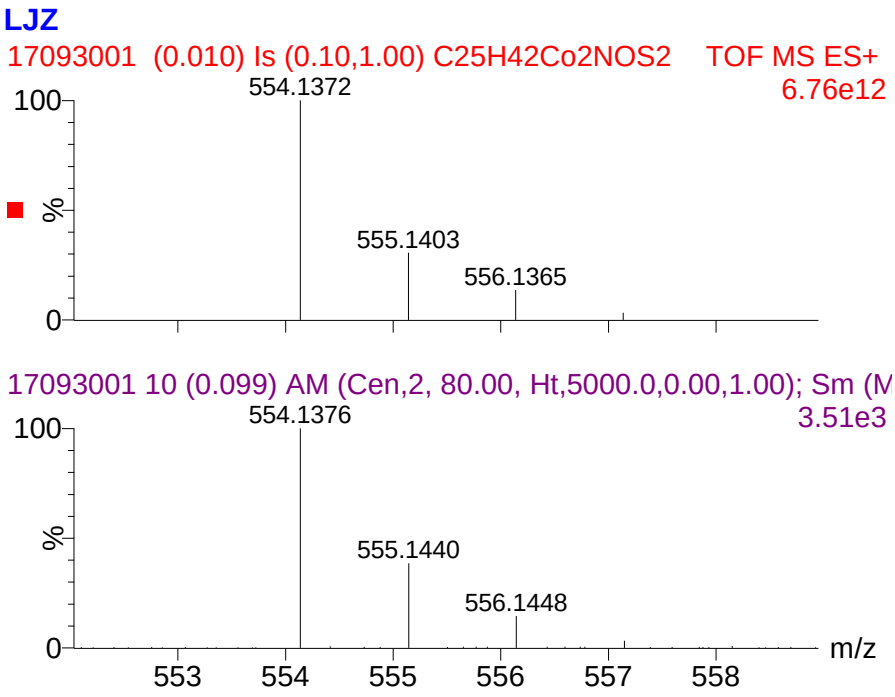

Fig. S16 ESI-HRMS of **3** in CH_2Cl_2.

(a) The signals at *m/z* = 654.0547 and 637.0283 correspond to $[\mathbf{3}-I]^+$ and $[\mathbf{3}-I-NH_3]^+$, respectively. (b) Calculated isotopic distribution for $[\mathbf{3}-I]^+$ (upper) and the amplifying diagram for $[\mathbf{3}-I]^+$ (bottom). (c) Calculated isotopic distribution for $[\mathbf{3}-I-NH_3]^+$ (upper) and the amplifying diagram for $[\mathbf{3}-I-NH_3]^+$ (bottom).

(a)

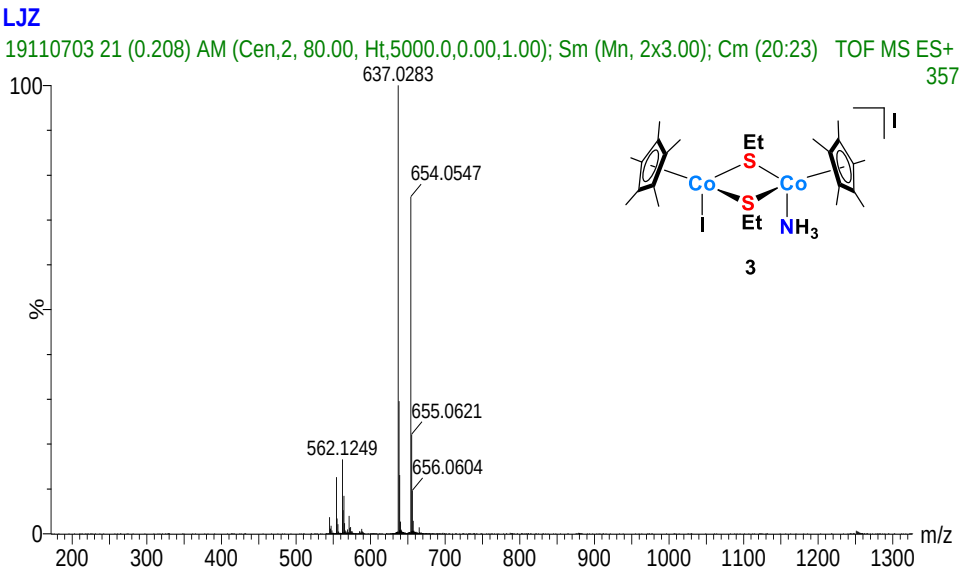

(b)

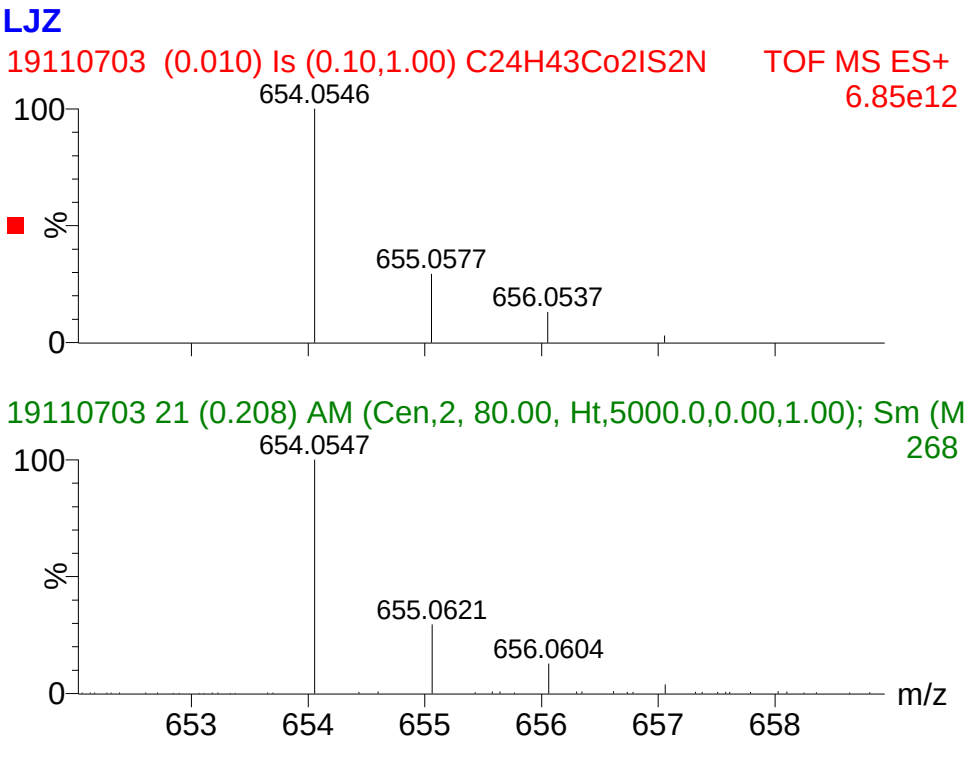

(c)

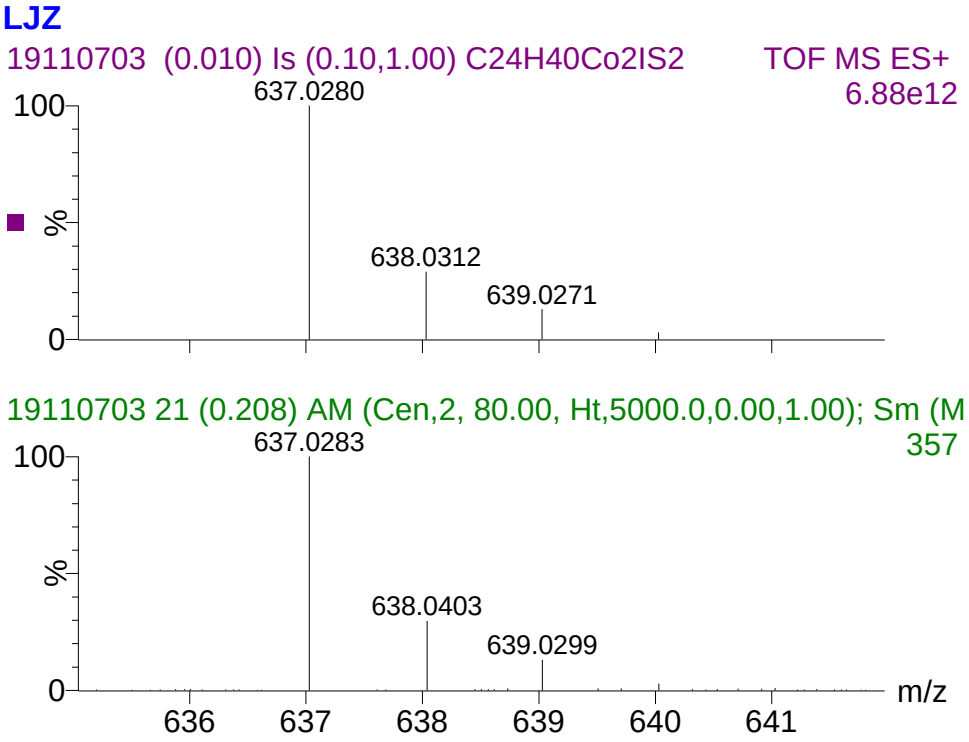
LJZ
19110703 (0.010) Is (0.10,1.00) C24H40Co2IS2
TOF MS ES+
6.88e12
637.0280
638.0312
639.0271
100
%
0
19110703 21 (0.208) AM (Cen,2, 80.00, Ht,5000.0,0.00,1.00); Sm (M
357
637.0283
638.0403
639.0299
636
637
638
639
640
641
m/z

Fig. S17 ESI-HRMS of D-**3** in CH_2Cl_2.

(a) The signal at *m/z* = 657.0740 corresponds to [D-**3**−I]$^+$. (b) Calculated isotopic distribution for [D-**3**−I]$^+$ (upper) and the amplifying diagram for [D-**3**−I]$^+$ (bottom).

(a)

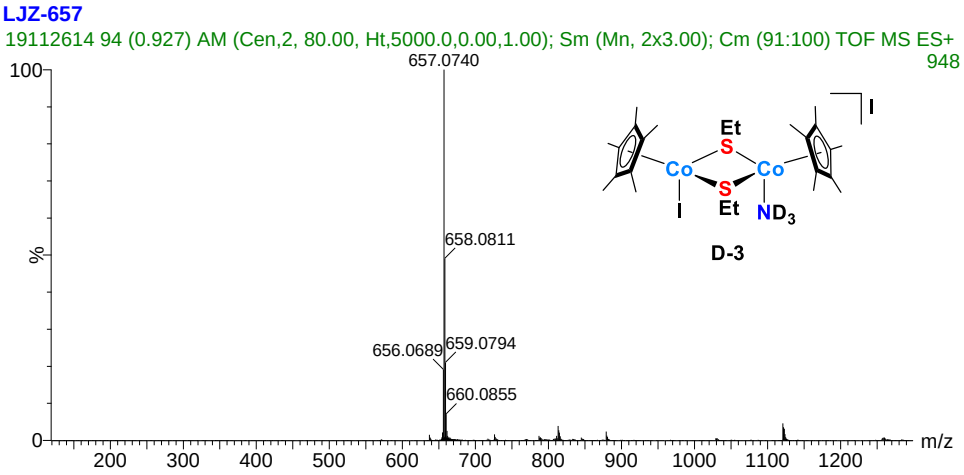

(b)

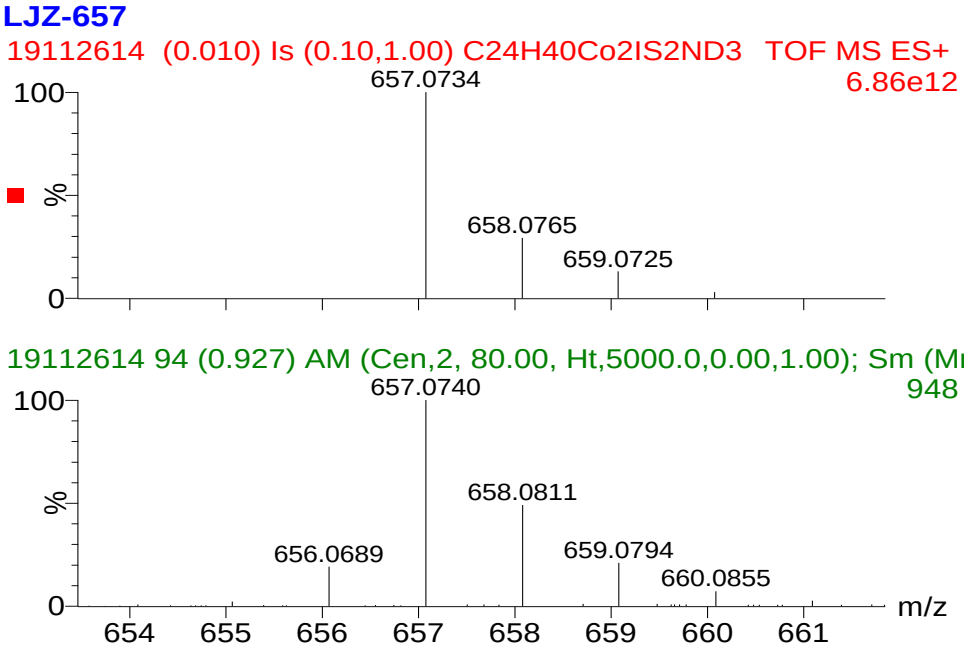

Fig. S18 ESI-HRMS of **4** in CH_2Cl_2.

(a) The signals at *m/z* = 284.0881, 275.5739 and 255.0619 correspond to $[\mathbf{4}-2(PF_6)]^{2+}$, $[\mathbf{4}-2(PF_6)-NH_3]^{2+}$ and $[\mathbf{4}-2(PF_6)-NH_3-MeCN]^{2+}$. (b) Calculated isotopic distribution for $[\mathbf{4}-2(PF_6)]^{2+}$ (upper) and the amplifying diagram for $[\mathbf{4}-2(PF_6)]^{2+}$ (bottom). (c) Calculated isotopic distribution for $[\mathbf{4}-2(PF_6)-NH_3]^{2+}$ (upper) and the amplifying diagram for $[\mathbf{4}-2(PF_6)-NH_3]^{2+}$ (bottom). (d) Calculated isotopic distribution for $[\mathbf{4}-2(PF_6)-NH_3-MeCN]^{2+}$ (upper) and the amplifying diagram for $[\mathbf{4}-2(PF_6)-NH_3-MeCN]^{2+}$ (bottom).

(a)

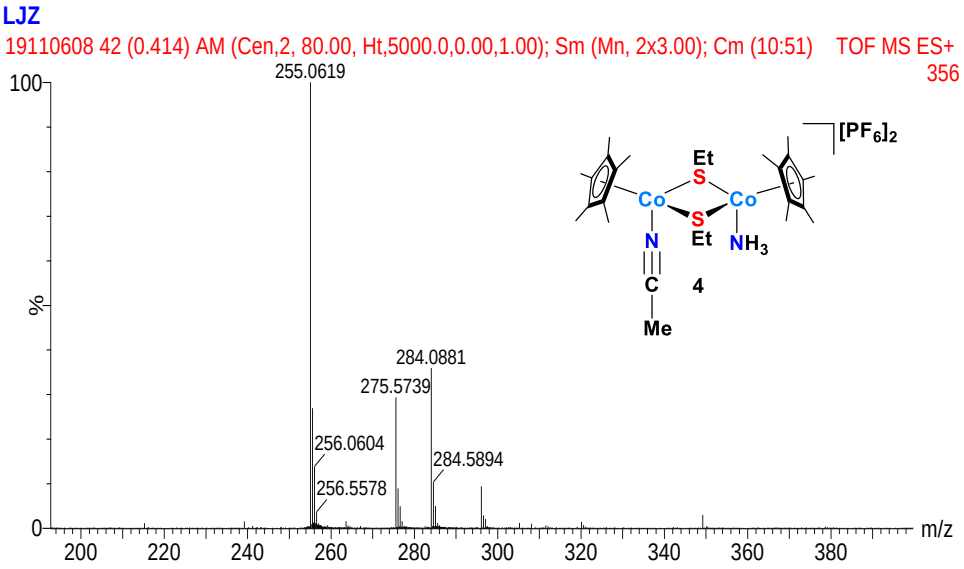

(b)

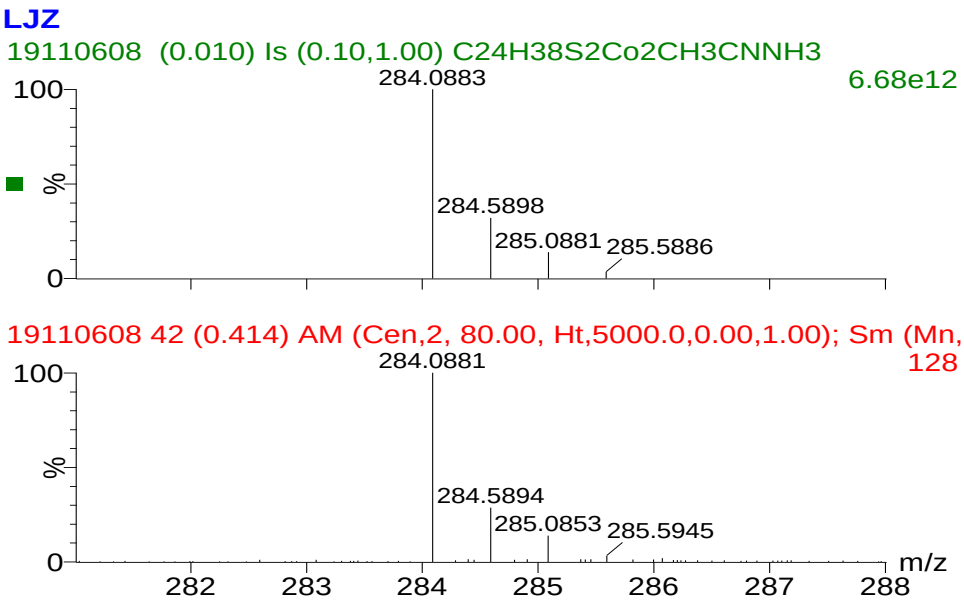

(c)

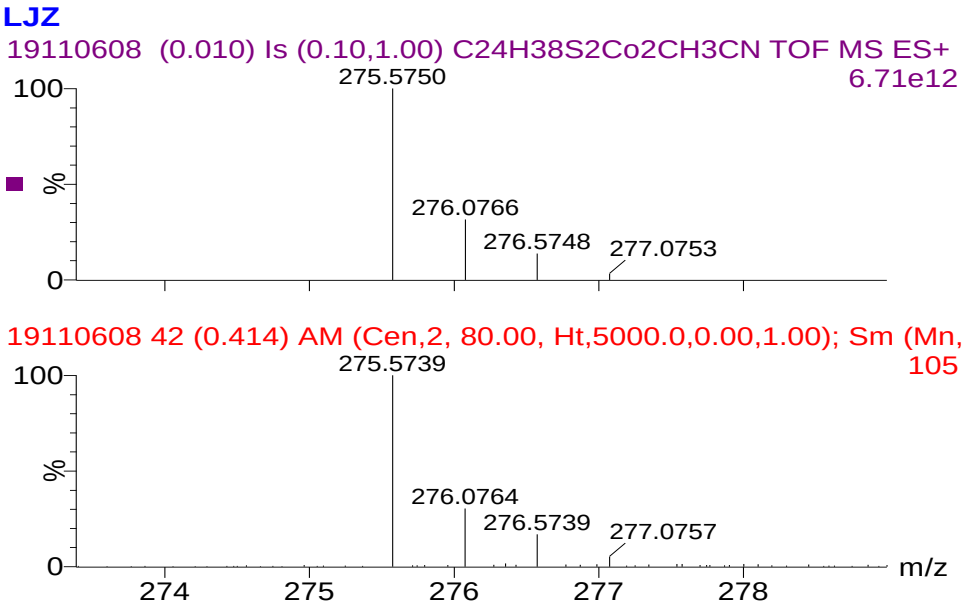
LJZ
19110608 (0.010) Is (0.10,1.00) C24H38S2Co2CH3CN TOF MS ES+
6.71e12
275.5750
276.0766
276.5748
277.0753
100
%
0
19110608 42 (0.414) AM (Cen,2, 80.00, Ht,5000.0,0.00,1.00); Sm (Mn,
105
275.5739
276.0764
276.5739
277.0757
m/z
274
275
276
277
278

(d)

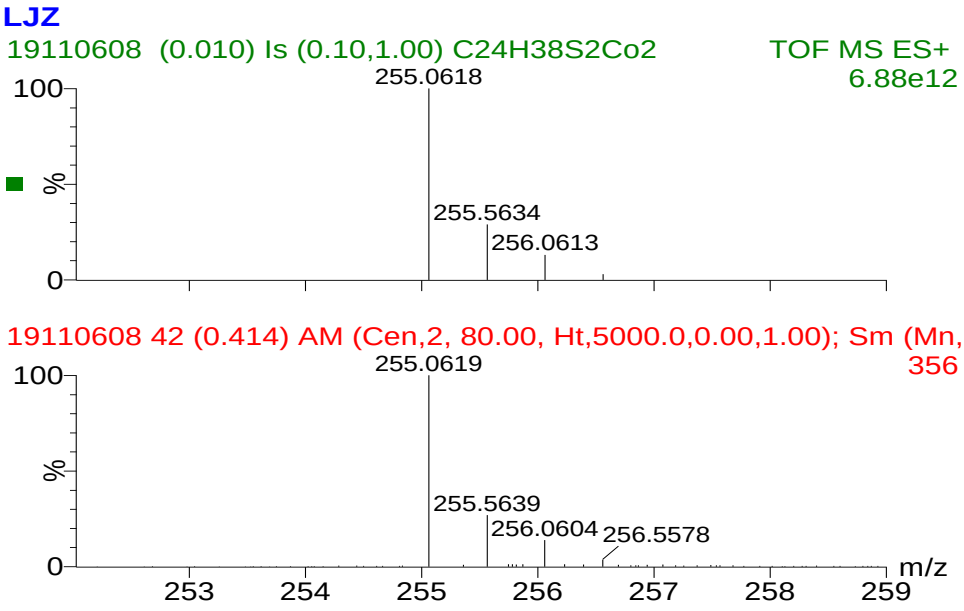
LJZ
19110608 (0.010) Is (0.10,1.00) C24H38S2Co2
TOF MS ES+
6.88e12
255.0618
255.5634
256.0613
100
%
0
19110608 42 (0.414) AM (Cen,2, 80.00, Ht,5000.0,0.00,1.00); Sm (Mn,
356
255.0619
255.5639
256.0604
256.5578
m/z
253
254
255
256
257
258
259

Fig. S19 ESI-HRMS of **5** in CH_2Cl_2.

(a) The signal at *m/z* = 567.1686 corresponds to $[\mathbf{5}-PF_6]^+$. (b) Calculated isotopic distribution for $[\mathbf{5}-PF_6]^+$ (upper) and the amplifying diagram for $[\mathbf{5}-PF_6]^+$ (bottom).

(a)

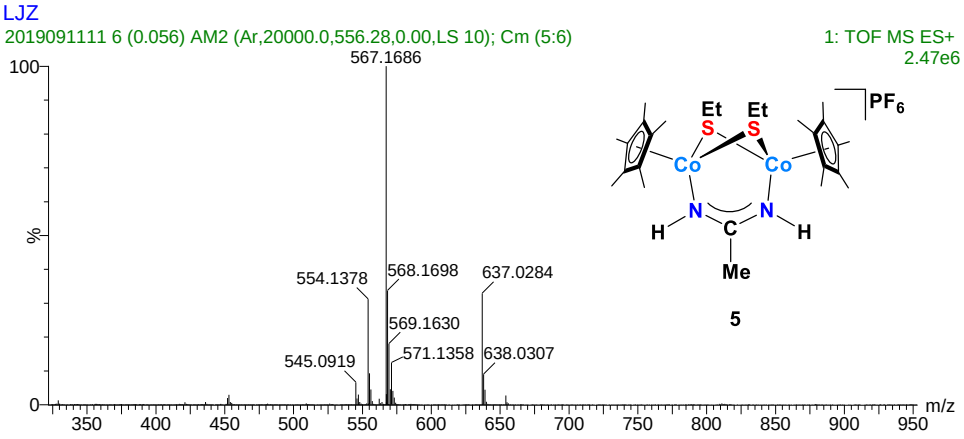

(b)

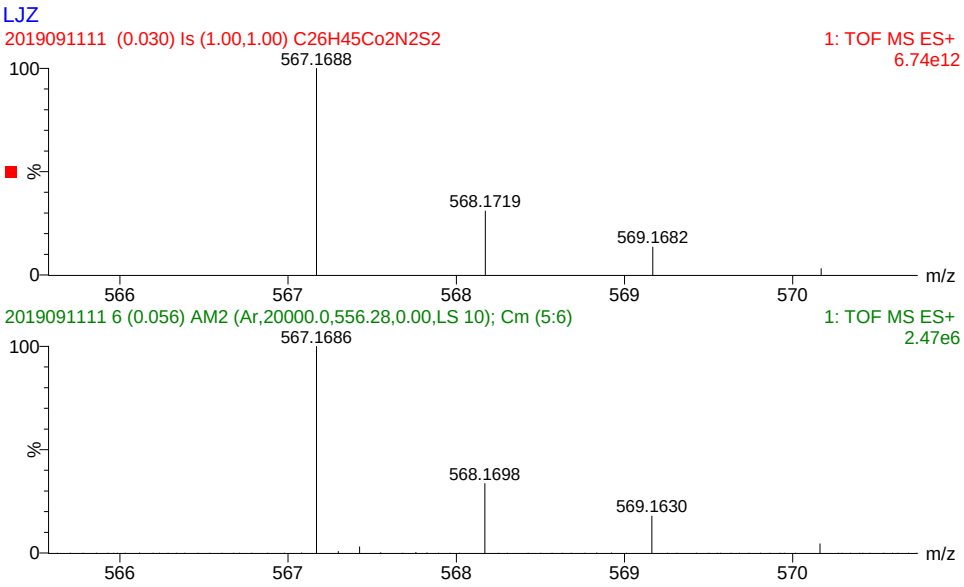

Fig. S20 ESI-HRMS of acetamidinium tetrafluoroborate in CH_2Cl_2.

The signal at an *m/z* = 59.0609 corresponds to $[MeC(NH_2)NH_2]^+$.

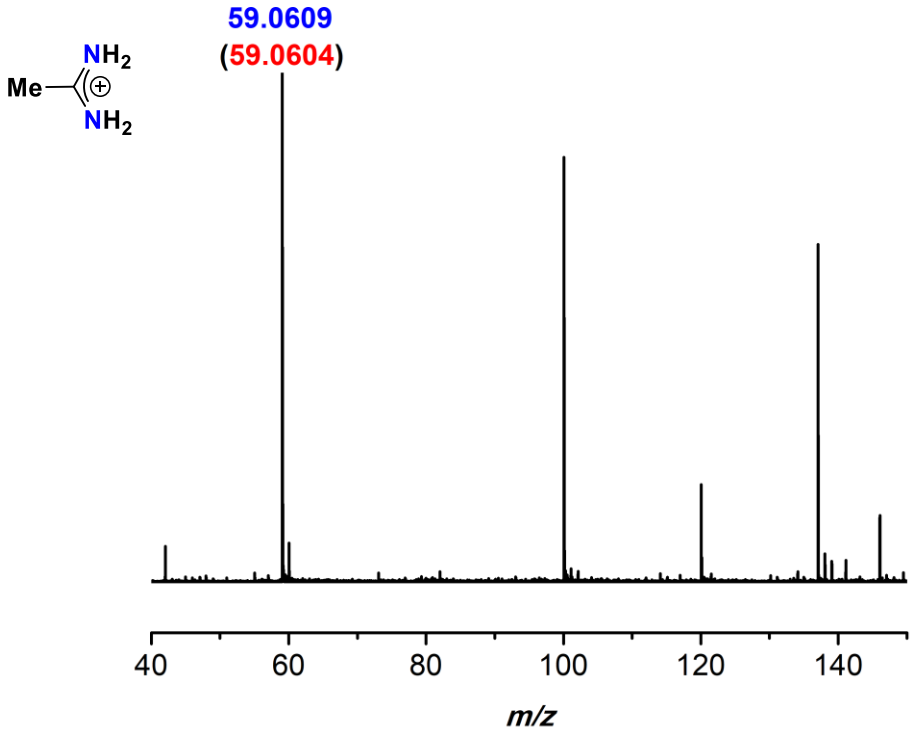

IV. IR spectra

Fig. S21 The IR (KBr) spectrum of **2**.

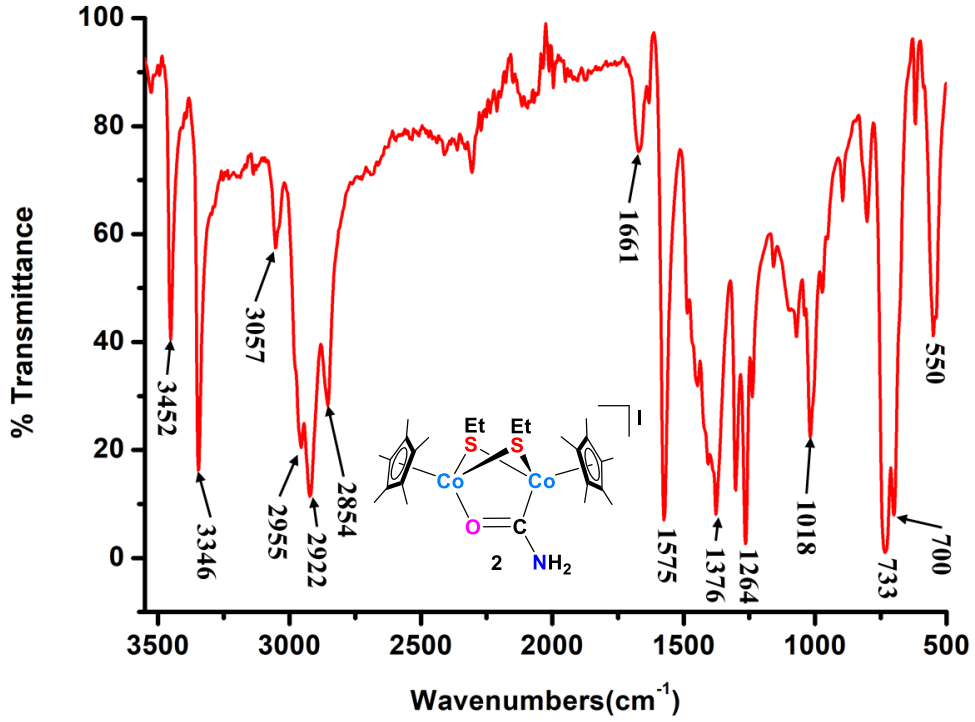

Fig. S22 The IR (KBr) spectrum of **3**.

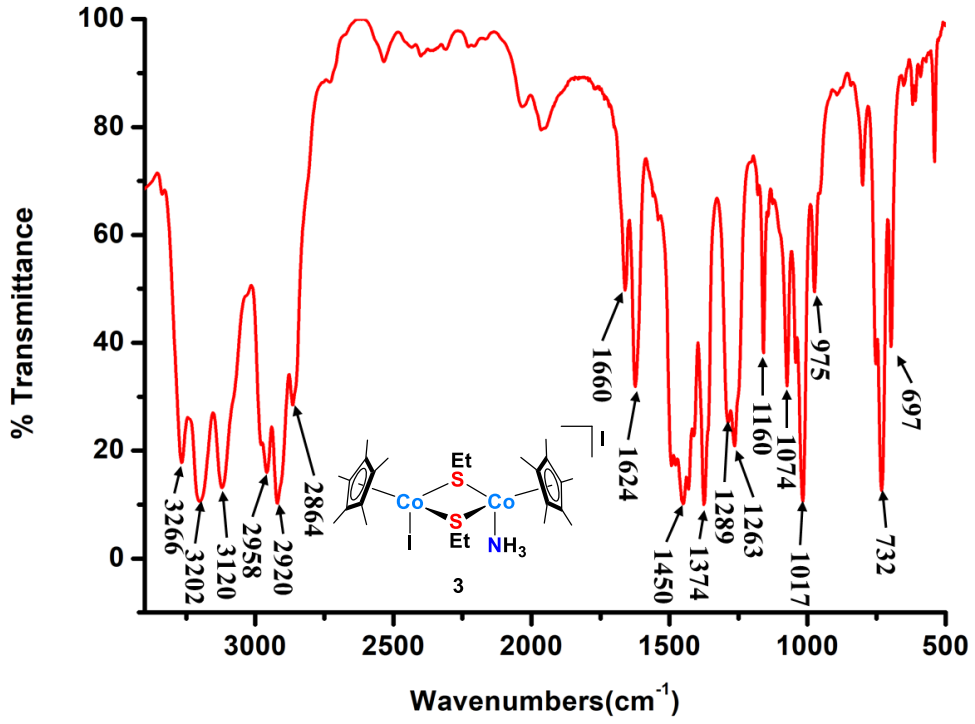

Fig. S23 The IR (KBr) spectrum of D-**3**.

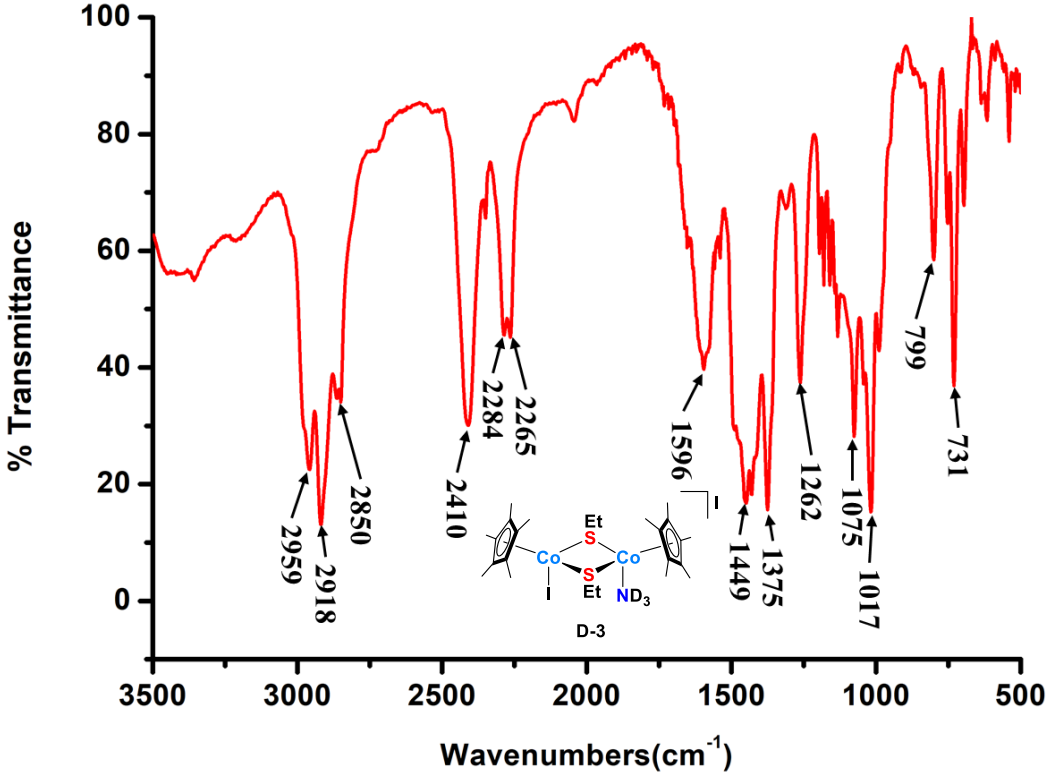

Fig. S24 The IR (KBr) spectrum of **4**.

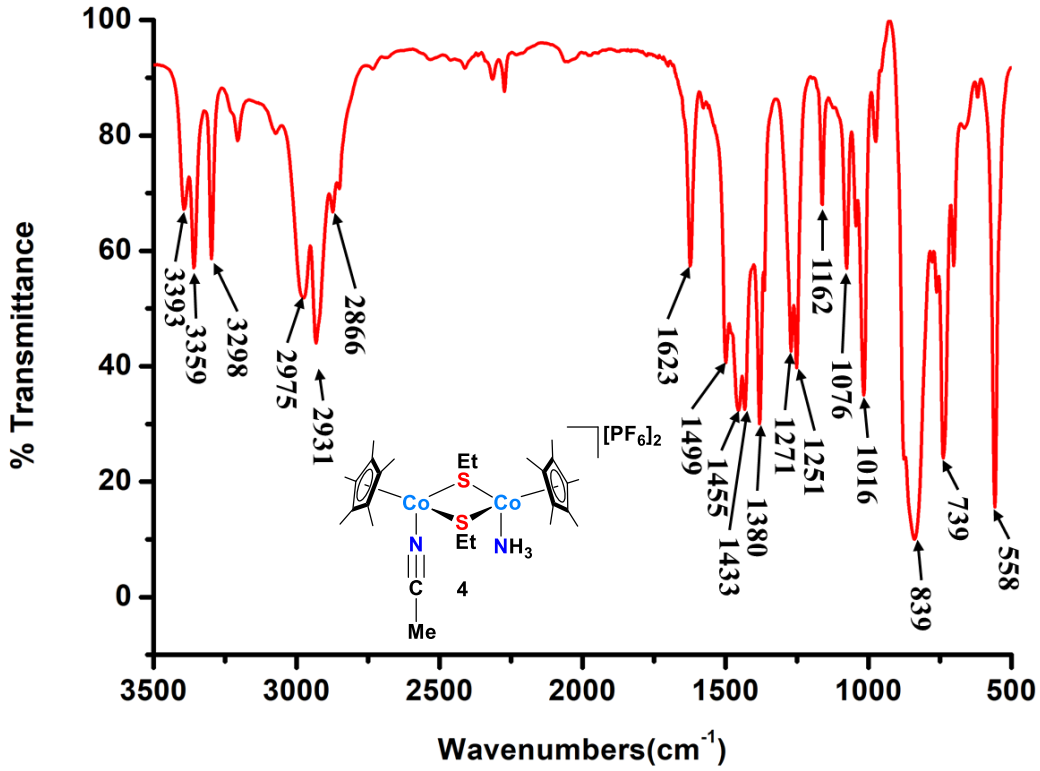

Fig. S25 The IR (KBr) spectrum of D-**4**.

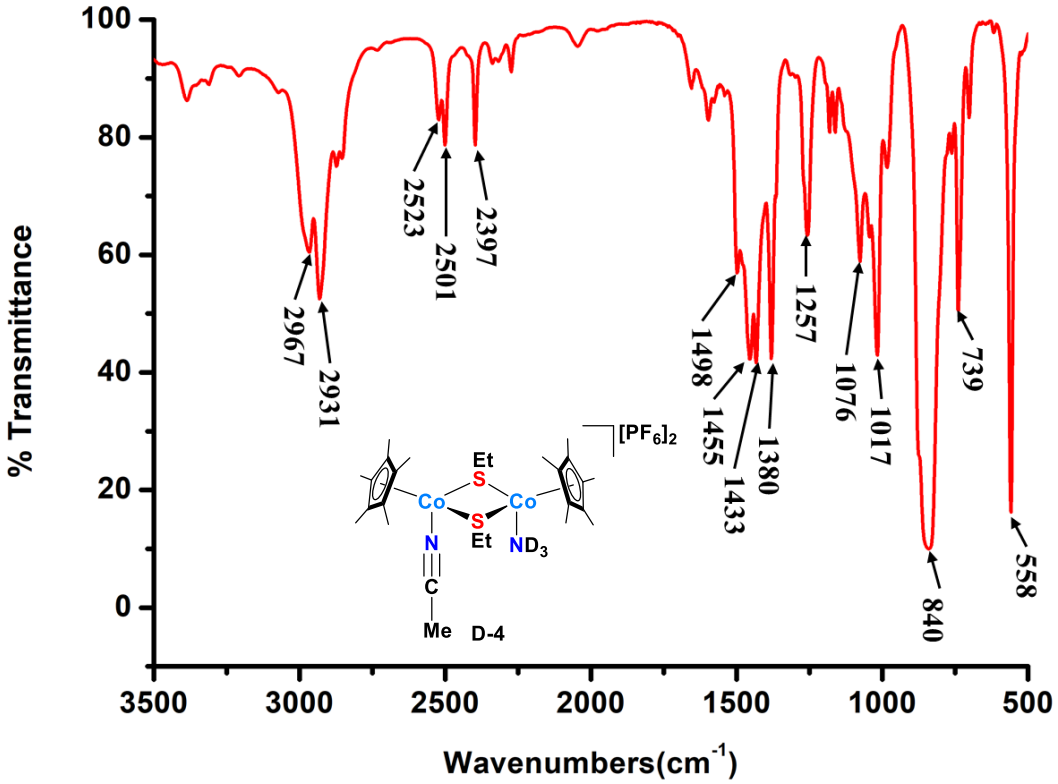

Fig. S26 The IR (KBr) spectrum of **5**.